COMPARATIVE WIND TUNNEL TESTS AT HIGH REYNOLDS NUMBERS OF NACA 64 621 AIRFOILS WITH TWO AILERON CONFIGURATIONS*

G. M. Gregorek

The Ohio State University
Columbus, Ohio 43220

ABSTRACT

An experimental program to measure the aerodynamic characteristics of the NACA 64-621 airfoil when equipped with plain ailerons of 0.38 chord and 0.30 chord and with 0.38 chord balanced aileron has been conducted in the pressurized O.S.U. 6" x 12" High Reynolds Number Wind Tunnel. Surface pressures were measured and integrated to yield lift and pressure drag coefficients for angles of attack from -3^o to $+42^o$ and for selected aileron deflections from 0^o to -90^o at nominal Mach and Reynolds numbers of 0.25 and 5×10^6. When resolved into thrust coefficient for wind turbine aerodynamic control applications, the data indicated the anticipated decrease in thrust coefficient with negative aileron deflection at low angles of attack; however, as angle of attack increased, thrust coefficients eventually became positive. All aileron configurations, even at -90^o deflections showed this trend. Hinge moments for each configuration complete the data set.

NOMENCLATURE

C_D	Drag coefficient, D/qc(1)
C_H	Hinge moment coefficient, H/qc_A^2 (1)
C_L	Lift coefficient, L/qc(1)
C_P	Pressure coefficient, $P - P_\infty/q$
C_T	Thrust coefficient, $C_T = C_L \sin\alpha - C_D \cos\alpha$
c	Airfoil chord
c_A	Aileron chord
M	Mach number
P	Surface pressure
P_∞	Free stream pressure
q	Dynamic pressure, $q = \frac{1}{2}\rho V^2$
Re	Reynolds number, $Re = \rho Vc/\mu$
α	Angle of attack
δ	Aileron deflection
ρ	Air density
x/c	Nondimensional chordwise coordinate
y/c	Nondimensional normal coordinate

INTRODUCTION

Aerodynamic controls have been used on wind turbine machines, both to modulate power and to brake the rotor during high wind conditions. As wind turbines increase in size, an aileron type of control becomes attractive. Although ailerons have been effectively used on aircraft for many years, the technical literature applicable to the wind turbine and upon which to base an aileron control system is sparse. The specialized wind turbine needs for data on thick airfoils operating at angles of attack above stall and with large negative aileron deflections are not available. This paper presents the results of an experimental program to expand the data base for aileron control of wind turbines.

A thick airfoil that is a candidate for wind turbine application is the NACA 64-621 section. The present program used this airfoil and fabricated, for testing, two dimensional models with plain ailerons of 0.38 chord and 0.30 chord and an aerodynamically balanced aileron of 0.38 chord. The models were evaluated in The Ohio State University 6" x 12" pressurized wind tunnel at nominal Mach number of 0.25 and Reynolds number, based on the 4" model chord, of 5×10^6. Surface pressures were measured, which when integrated, produced lift, pressure drag and moment coefficients. The angle of attack ranged from -3^o to $+42^o$ and the aileron deflections were 0^o, -10^o, -15^o, -30^o, -45^o and -90^o for the 0.38c plain aileron and 0^o, -15^o, -30^o, and -90^o for the other two ailerons. The surface pressures of each aileron configuration were integrated to yield the hinge moment as a function of angle of attack and deflection.

EXPERIMENTAL FACILITIES

The O.S.U. 6" x 12" High Reynolds Number Wind Tunnel shown in Figure 1 is a two-dimensional facility designed specifically to test airfoils near full scale Reynolds numbers. It is a pressurized, blow down, wind tunnel equipped with an advanced data processing system, and capable of operating at stagnation pressures near 500 psia and at Mach numbers from 0.2 to 1.1.

In a typical test run of 15 seconds duration, surface pressures are obtained at one angle of attack, one Reynolds number and one Mach number. An on-line computer controls the test sequence once the air supply valve is opened, actuating pressure cut-off valves at the desired test condition, initiating a pitot probe traverse of the wake one chord downstream of the model, and closing the air supply valve on completion of the wake traverse. The 48 port scannivalve/cut-off valves shown in Figure 2 trap the surface pressures for sampling after tunnel shut down. A Harris Slash 6 computer processes the electrical signal from the trapped pressures to engineering format, and the test results in the form of C_p vs x/c, integrated lift, drag, and pitching moment coefficients are displayed on the data operator's CRT. The raw data is stored on magnetic tape for a permanent record and the processed information made into hard copy plots and printouts. The next test cycle can be set up; depending upon the required air supply, 40 or more such test runs can be made per day.

*Presented at the Horizontal-Axis Wind Turbine Technology Workshop, May 8-10, 1984 in Cleveland, Ohio. Supported by NASA Lewis Rsch Cntr, Grant NAG 3-330.

The models are mounted to circular plates that fit flush into the wind tunnel side walls as illustrated in Figure 3. With multi-element models, the main element mounts to a rectangular cut-out in this disc; model angle of attack is changed by rotating this disc. The aileron is fitted into a small disc that sets into the main circular plate. The small disc has its center at the hinge location so that the aileron can be rotated about the hinge line independent of the main element angle of attack. With these two separate mounting discs, model main element angle of attack can be varied from 0^0 to 360^0 and aileron deflection can be varied similarly. For the present model tests, with the hinge located on the upper surface of the airfoil, aileron deflections of 0^0 to -100^0 are possible.

The model airfoils are presented in Figure 4. They have a 4 inch chord and 6 inch span and are cast from precision molds of aluminum-epoxy material. To sustain the high airloads when deflected -90^0, the ailerons had graphite roving distributed internally. The pressure taps were formed into the main element and flap during the molding process.

The airfoil and the three aileron contours are presented in Figure 5. The location of the hinge lines are given in terms of non-dimensional coordinates as $x/c = 0.635$, $y/c = 0.0825$ for both 0.38 chord models and as $x/c = 0.712$ and $y/c = 0.0677$ for the 0.30 chord aileron.

RESULTS AND DISCUSSION

The wind tunnel test program consisted of more than 100 runs at nominal Mach number of 0.25 and Reynolds number of 5×10^6, with the major part of the program focussed upon the 0.38c plain aileron. Angles of attack from -9^0 to $+45^0$ were examined for this configuration at five aileron deflections ranging from 0^0 to -90^0. Limited tests of the other two aileron configurations - the 0.38c balanced aileron and the 0.30c plain aileron - were made at selected test conditions; the purpose of these tests were to evaluate the effects of aerodynamic balance and changing chord length by comparing the results with the 0.38c plain aileron baseline. All models had two dimensional trip strips of 0.002 inch (.0005c) located at .05c on the upper and lower surfaces to assure a turbulent model boundary layer.

Pressure Distributions

Three pressure distributions typical of those measured on the 0.38c plain aileron are presented in Figure 6 to illustrate the change in pressure distribution with angle of attack when aileron deflection is fixed at zero degrees. The square symbols represent the pressure coefficients on the upper surface, the diamond symbols, the lower surface pressure coefficients. The main element pressures are plotted from $x/c = 0$ to 0.60 while the aileron pressure are displayed from $x/c = 1.00$ to 1.40; this displacement of the aileron pressure distribution has been performed to distinguish between the pressures on the aft face of the main element and on the forward face of the aileron.

The distributions of Figure 6 show that as angle of attack increases from 0^0 to 18^0 lift coefficient increases from $C_\ell = 0.38$ to $C_L = 1.18$. The plateau in the aileron pressures in Figure 6b indicates the flow has separated entirely on the upper aileron surface and the lift coefficient has reached $C_\ell = 1.0$ at 9^0 angle of attack. When the angle of attack is doubled to 18^0, the lift has increased only to $C_\ell = 1.18$ while the separated zone has moved forward to the main element and has reached $x/c = 0.40$

Figure 7 indicates the pressure distributions obtained on the 0.38c plain aileron at a fixed angle of attack when the aileron is deflected trailing edge up. As the aileron is deflected from 0^0 to -15^0 and then to -30^0, lift coefficient at fixed angle of attack of 9^0 decreases from $C_\ell = 1.00$ to 0.35 and finally to $C = -0.02$. Of interest is the complete change of pressure distribution on the aileron as it is deflected. The low negative pressure coefficients of the separated upper aileron surface increase to positive values as the aileron deflects, while the lower surface pressure coefficients, initially positive become negative. The pressure plateau of Figure 7c shows that the lower surface of the aileron has now separated. These pressure changes, of course, result in the loss of lift measured, but also an increase in drag and a change in the aileron hinge moment. In fact, the hinge moment changes from a negative value- an aerodynamic moment that tends to move the aileron trailing edge up - to a positive hinge moment at the -30^0 deflection.

The pressure distributions obtained from the 0.38c balanced and 0.30c plain aileron are compared with the baseline 0.38c plain aileron at 18^0 angle of attack and -30^0 aileron deflection. At 18^0, the baseline aileron lift has increased to $C_\ell = 0.89$ from the -0.02 shown at angle of attack 9 in Figure 7c. The 0.38c balanced aileron has a higher lift, $C_\ell = 1.03$, than the baseline, mainly due to the ability of the balanced aileron to influence the main element surface pressures, spreading the upper and lower pressures to increase lift. In the same manner, the smaller chord 0.30c plain aileron has the lowest lift, $C_\ell = 0.71$, due to the inability of the aileron to alter the main element pressures.

These pressure distributions and the integrated lift coefficients follow trends established by earlier airfoil tests at modest angles of attack. Even when the aileron is deflected at extreme angles, -90^0, for example, the distributions, though irregular in appearance, are rational. Figure 9 illustrates the pressure distribution for the 0.38 plain and balanced ailerons at 18^0 angle of attack and -90^0 aileron deflection. The large negative deflection has accelerated the flow on the lower surface so that it has low pressure surface (the square symbols are the upper surface C_p). Further, the aileron is carrying a high positive hinge moment with high pressure on the forward (upper) surface and a low pressure on the aft (lower) surface. These extreme conditions at angle of attack lead to large negative lift coefficients for both aileron configurtions, $C_\ell = -0.89$ and $C_\ell = -0.57$ for the plain and balanced configurations, respectively.

When the angle of attack is increased from 18^0 to 36^0 for this extreme negative aileron deflection of -90^0, the pressure distributions proceed through a drastic change. Figure 10 compares the distributions measured at these two angles of attack for the baseline 0.38c plain aileron.

As shown in Figure 10b for 36° angle of attack, the upper surface of the main element is now the low pressur surface; it is essentially flat, indicating it lies in a separated zone. The lower surface, at 18° angle of attack the low pressure region, now is the high pressure surface. Similarly, the upper aileron surface has low pressure coefficients and of the same order as the main element pressure coefficients, while the lower aileron surface has a higher (though still negative) pressure coefficient. The net result of this pressure distribution is that the lift coefficient has increased from C_ℓ = -0.89 to C_ℓ = +0.70 as angle of attack changed from 18° to 36°.

This somewhat surprising behavior of the NACA 64-621 airfoil with ailerons deflected to large negative deflections producing substantial positive lift when at angles of attack above stall was duplicated by all three aileron configurations tested. The impact of this post-stall behavior on the other aerodynamic characteristics of the aileron configurations is treated next.

Aerodynamic Characteristics

Each of the surface pressure distributions obtained in the test program were integrated to determine a normal and an axial coefficient for the main element and aileron. These component coefficients were then resolved into a total two dimensional lift and drag coefficient based on airfoil chord. An axial thrust coefficient, C_T defined as

$$C_T = C_\ell \sin\alpha - C_d \cos\alpha \qquad (1)$$

was formulated from the resulting lift and drag coefficients.

These three aerodynamic characteristics are displayed as a function of angle of attack for the 0.38c plain aileron in Figure 11. The maximum lift coefficient is observed to decrease from C_ℓ = 1.22 when δ_A = 0° to C_ℓ = 1.0 and C_ℓ = 0.83 as aileron deflection increases to -10° and -15°. At δ_A = -45°, the maximum lift has recovered to C_ℓ = 1.0 when angle of attack has increased to 27° while an aileron deflection of -90° leads to a maximum C_ℓ = 0.7 at 36° angle of attack. The lift curve slopes for aileron deflections less than 30° are noted to be linear below C_ℓ = 0.8.

At aileron deflections below -30°, the drag coefficients show a generally parabolic form, increasing from C_d = 0.01 near zero angle of attack to C_d = 0.40 at angles near 24°. When the aileron is deflected to -45° and above, the drag decreases initially with angle of attack before starting to follow the parabolic upward trend. At -90°, for example, drag coefficient falls from C_D = 0.60 at zero to 0.32 at 33° angle of attack before starting to rise. This behavior is caused by the distribution of pressure noted earlier at high angles of attack and flap deflections; high pressures on the upper surface of the deflected aileron drop due to massive flow separation at high attack angles and the axial force on the aileron is reduced.

When these lift and drag characteristics are combined according to Equation (1), Figure 11c results. The positive values of C_t at low angles of attack and deflection are desirable and necessary to drive the rotor to produce power, however, for the rotor to decelerate in high wind conditions, the aileron deflections must generate negative thrust coefficients. For modest angles of attack, the large aileron deflections do, indeed, create substantial negative values as shown in Figure 11c. Thrust coefficients increase from C_t = -0.30 and C_t = -0.8 for the -45° and -90° deflections to zero at angles of attack of 19° and 33°, respectively. Above these angles, a region of positive thrust coefficients exist. The -45° deflection shows a peak C_t = 0.24 at 24° before decreasing to zero at 34° angle of attack; the -90° deflection has a maximum C_t = 0.14 at 36° angle of attack that decreases to zero beyond 45° angle of attack. These positive zones of thrust coefficient may reflect adversely upon the ability of this aileron configuration to brake the rotor.

The aerodynamic characteristics of the 0.38c balanced aileron are presented in Figure 12. The symbols are the experimental data; the broken lines represent the results at corresponding aileron deflections of the 0.38c plain aileron. The most striking point of Figure 12a is the large lift coefficient measured at the -90° aileron deflection, above C_ℓ = 1.2 at 32° angle of attack. In contrast, the peak lift coefficient for the plain aileron was C_ℓ = 0.7 at 36°. Further, the balanced aileron appears to decrease the angle of zero lift about 4°. The thrust coefficients displayed in Figure 12b indicate that the low aileron deflections produce low values of C_t than the corresponding C_t of the plain aileron, but the high lift of the -90° deflection decreases the effectiveness of the balanced aileron. Thrust coefficient becomes positive at 28° and peaks at C_t = 0.21 at 33° angle of attack.

Performance of the 0.30c plain aileron is shown in Figure 13. For the -90° aileron deflection, lift becomes positive at 24° angle of attack, reaching a maximum of C_ℓ = 0.9 at 33° angle of attack. The smaller chord plain aileron exhibits positive thrust coefficients at the -90° deflection as do the other two aileron configurations, crossing C_t = 0 at 27° angle of attack and peaking near C_t = 0.20 at 33° angle. The 0.30 plain aileron has less ability to generate negative thrust coefficients, C_t = -.4 compared to C_t = -0.75 of the 0.38 plain aileron, and can shift the angle of attack for zero thrust to 27° in contrast to the 33° angle for zero thrust of the larger chord plain aileron.

Hinge Moments

The pressures distributed on the aileron surfaces produce an aerodynamic moment about the hinge line, and knowledge of this moment is important when designing an aileron control system. By integrating the pressures measured on the aileron with respect to the hinge line, this aerodynamic hinge moment can be obtained. This moment is shown in coefficient form in Figure 14 for the 0.38c plain aileron where the hinge moment coefficient is defined by equation (2) below,

$$C_H = \frac{H}{q C_A^2} \qquad (2)$$

with a positive hinge moment defined as a moment tending to rotate the aileron trailing edge down. At low angles of attack and aileron deflection the hinge moment variations with increasing angle of attack and deflection. At high deflection angles the positive

hinge moment is almost independent of angle of attack until angles of attack above 20^0; hinge moment then decreases rapidly, changing sign at 24^0 and 32^0 angle of attack for the -45^0 and -90^0 aileron deflections, respectively.

Figure 15 indicates the hinge moments obtained on the balanced aileron and in the 0.30c plain aileron. As anticipated, the balanced aileron reduces the hinge moment for all cases when compared to the 0.38c plain aileron. Similarly, the hinge moment of the 0.30c plain aileron at -90^0 aileron deflection is lower than the baseline. All three configurations demonstrate the change in hinge moment sign at post stall angles of attack.

By cross plotting the hinge moment information, the angle to which the aileron will deflect to make the hinge moment zero may be obtained. The float angle is shown in Figure 16 as a function of angle of attack for the three aileron configurations.

SUMMARY

Three aileron configurations of the NACA 64-621 airfoil have been examined in the OSU 6" x 12" high Reynolds number wind tunnel at Mach number 0.25 and Reynolds number of 5×10^6 based on the 4 inch model chord. The purpose of the test was to contribute to the existing aerodynamic data base of candidate wind turbine airfoils and to measure the performance of the three aileron configurations at high angles of attack and aileron deflection to evaluate their suitability for wind turbine power modulation and braking.

Pressure distributions obtained on the 0.38c plain aileron; 0.38c balanced aileron and 0.30c plain aileron were integrated to obtain lift, drag and thrust coefficients at angles of attack to 45^0 and angles of aileron deflection to -90^0. Reduction of the data leads to the following observations:

i) At modest angles of attack all aileron configurations behaved normally, with both lift coefficient and thrust coefficient decreasing with increasing negative aileron deflection. Maximum lift coefficient decreased as well.

ii) At angles of attack above 20^0 and aileron deflections above -30^0 the pressure distributions indicated massive separation on the upper surface accompanied by low upper surface pressures, resulting in increasing positive lift.

iii) As a result of this lowered upper surface pressure at -90^0 aileron deflection, for example, positive thrust coefficients were measured at angles of attack above 33^0, 28^0, and 27^0 for the 0.38c plain, 0.38c balanced and 0.30c plain aileron, respectively. These regions of substantial positive thrust coefficients existed for more than 10^0 for all configurations.

iv) Use of aileron deflection as a power modulation method is feasible, and as an aerodynamic braking system is possible when angles of attack can be limited to those producing negative thrust coefficients. The 0.38c plain aileron was most successful as a brake, followed by the 0.38c balanced aileron and the 0.30c plain aileron.

v) Hinge moments measured on the three configurations were maximum for the 0.38c plain aileron, with the balanced 0.38c aileron airfoil less.

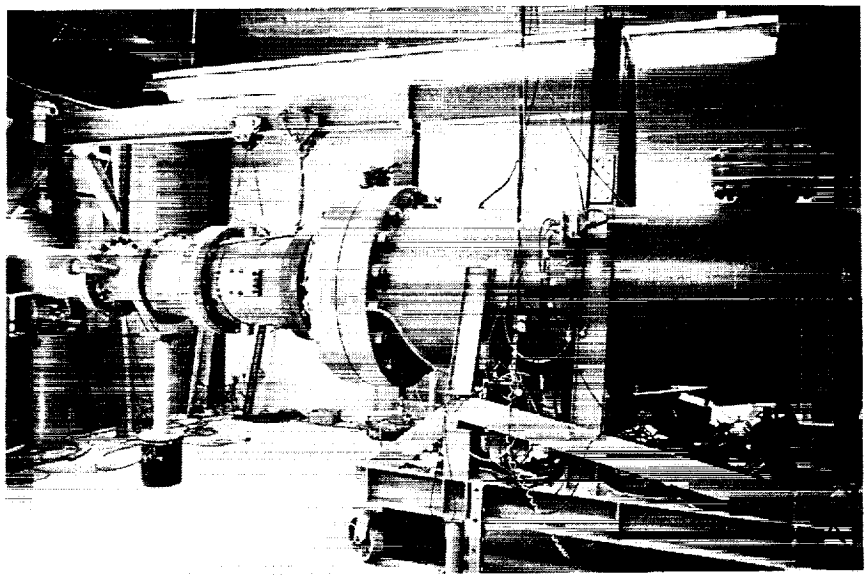

FIGURE 1. The OSU Pressurized 6" x 12" Airfoil Wind Tunnel.

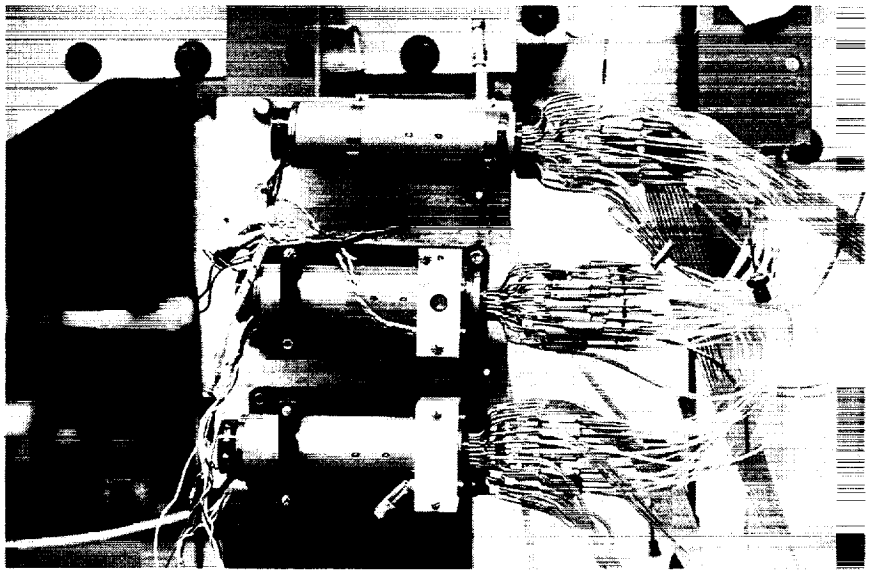

FIGURE 2. Scanning Valve/Lock Valves For Pressure Sensing.

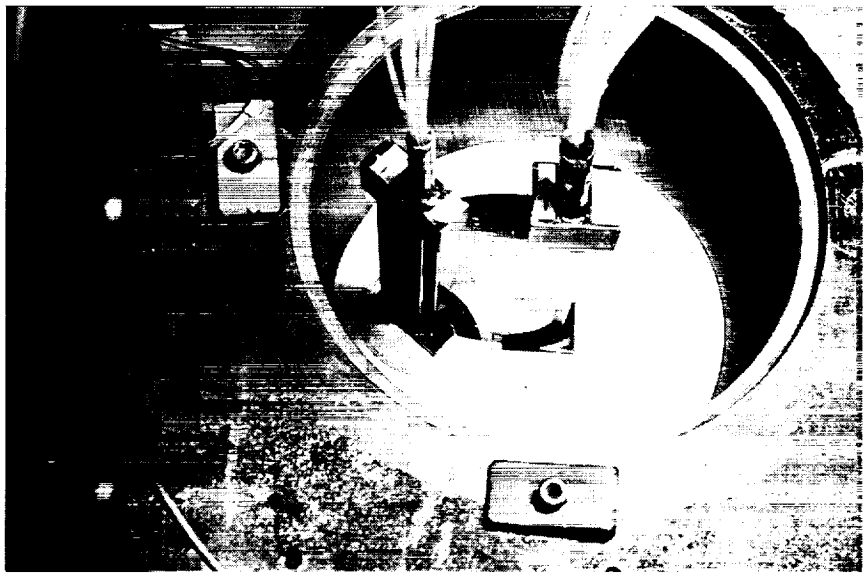

FIGURE 3. Model Installed in Wind Tunnel.

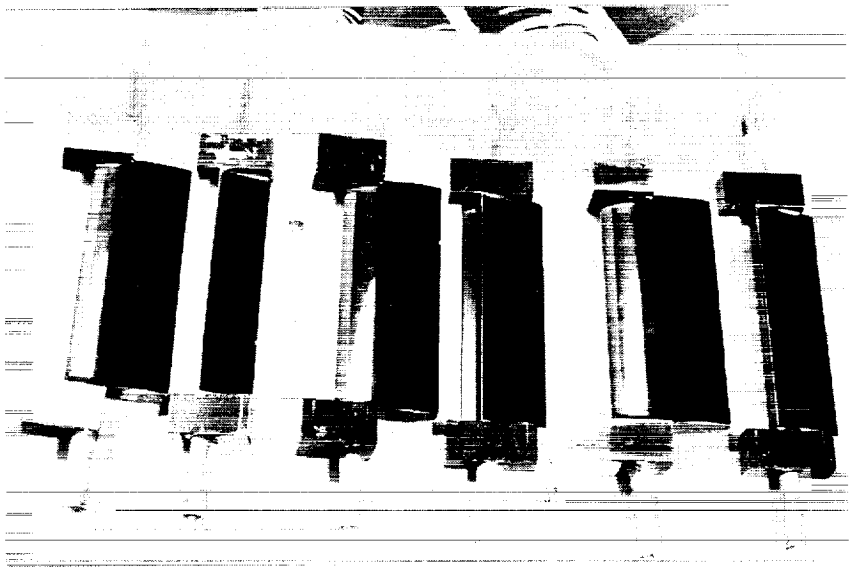

FIGURE 4. The 0.30c Plain, 0.38c Balanced and 0.38c Plain Aileron Models.

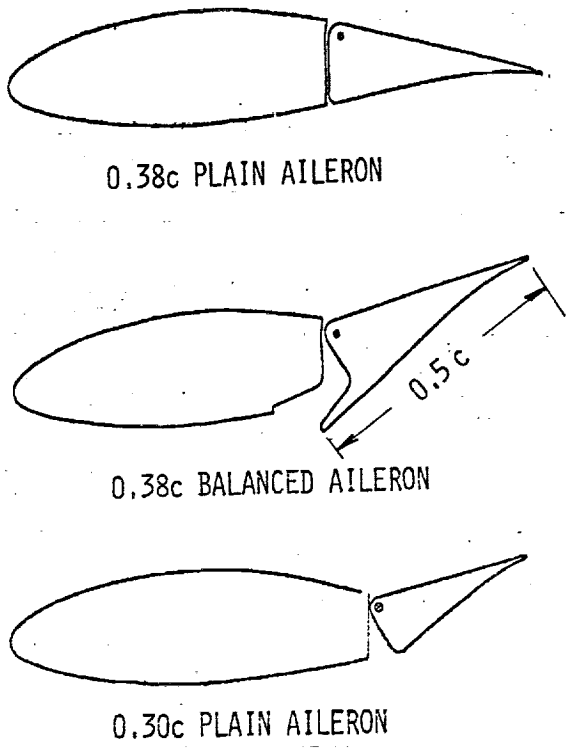

FIGURE 5. NACA 64 621 Airfoils With The Aileron Configurations Tested.

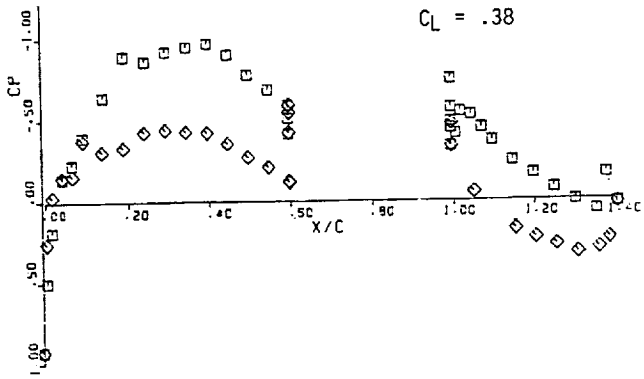

a) 0^0 Angle of Attack

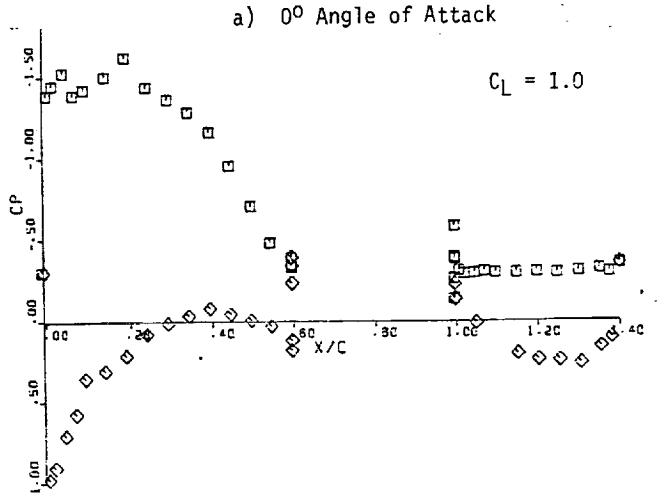

a) 9^0 Angle of Attack

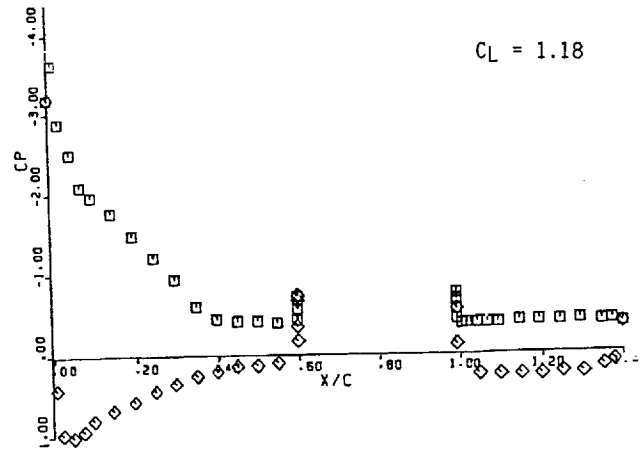

c) 18^0 Angle of Attack

FIGURE 6. Pressure Distribution on 0.38c Plain Aileron With Aileron Deflection 0^0 and Angle of Attack 0^0, 9^0, and 18^0.

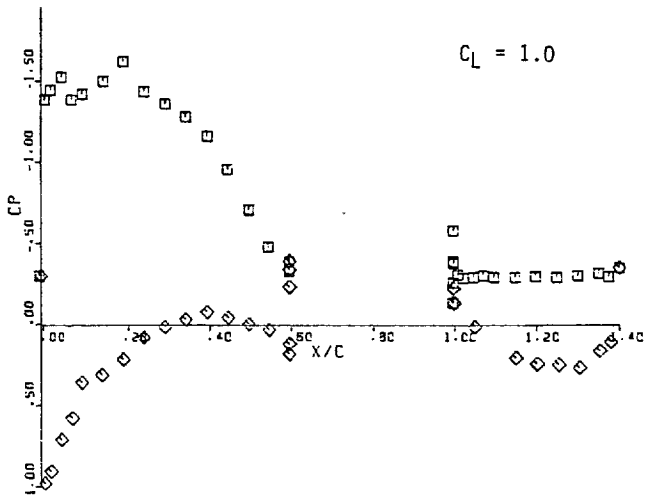

a) 0^0 Aileron Deflection

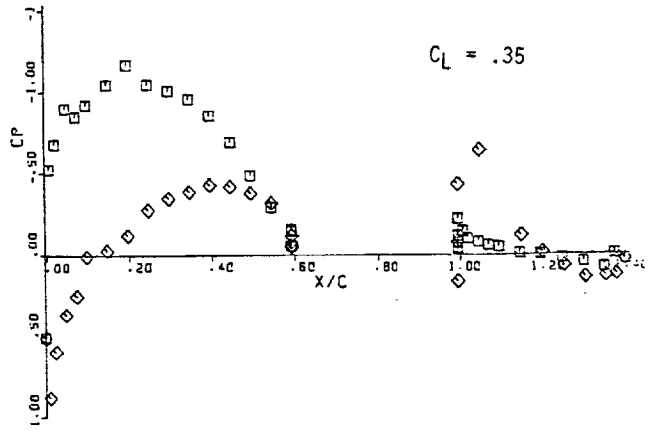

b) -15^0 Aileron Deflection

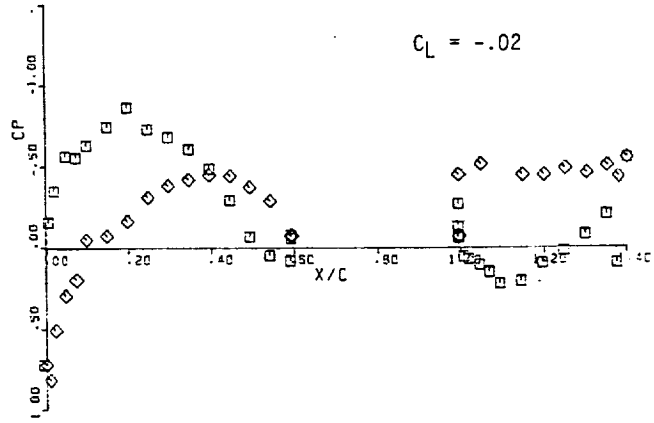

b) -30^0 Aileron Deflection

FIGURE 7. Pressure Distribution on 0.38c Plain Aileron at 9^0 Angle of Attack and Aileron Deflections 0^0, -15^0 and -30^0.

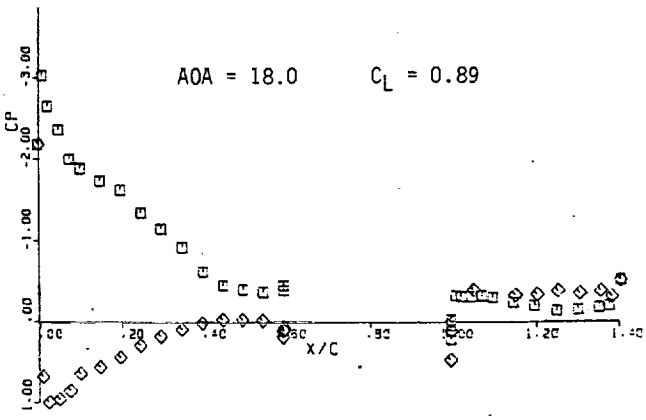

a) 0.38c Plain Aileron

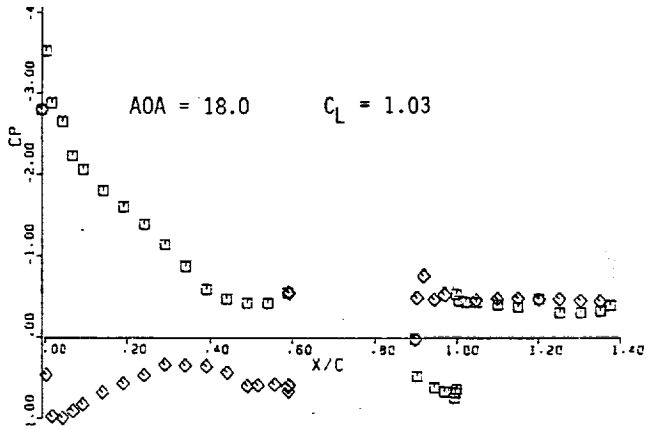

b) Balanced Aileron

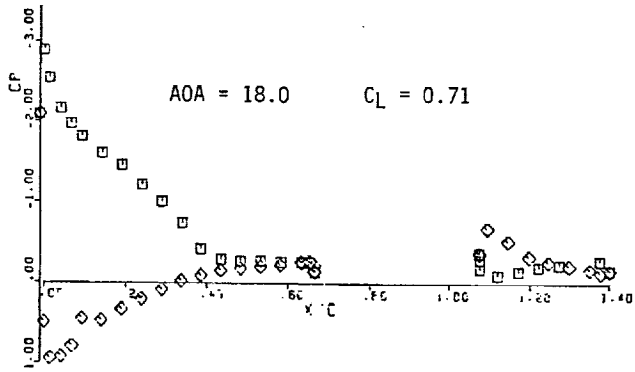

c) 0.30 Plain Aileron

FIGURE 8. Pressure Distribution on the Three Configurations at 18° Angle of Attack and Aileron Deflection -30°.

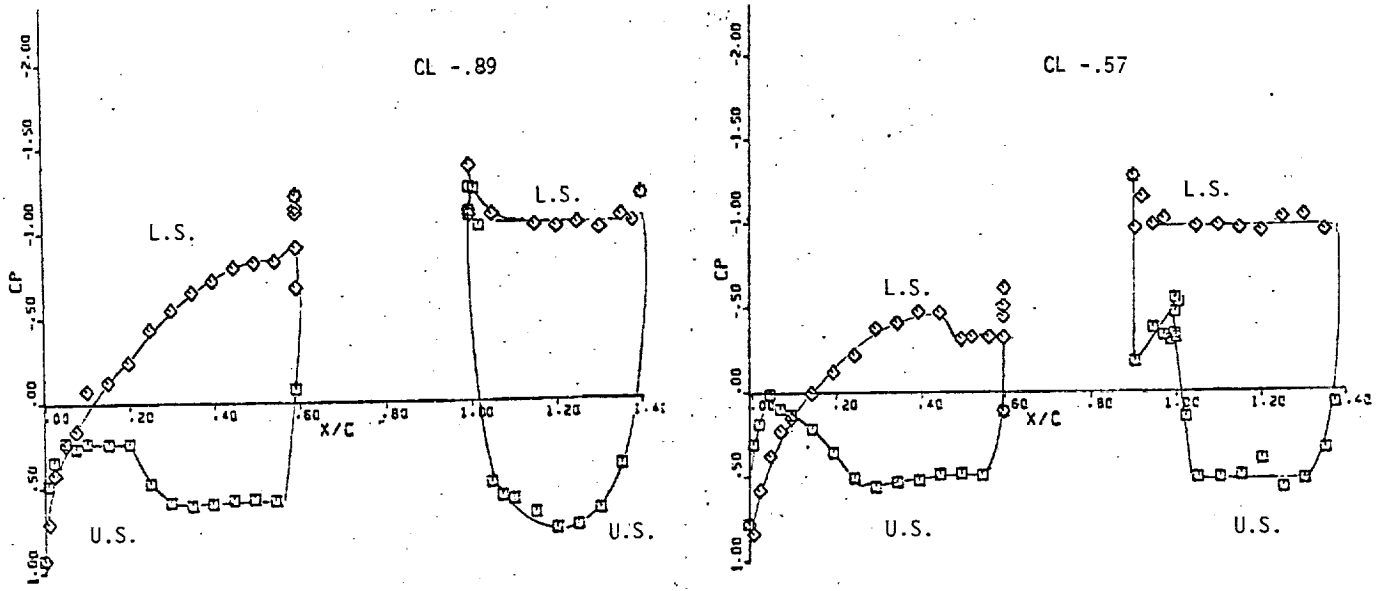

a) 0.38c Plain Aileron

b) 0.38c Balanced Aileron

FIGURE 9. Pressure Distribution on Plain and Balanced 0.38c Aileron at 18° Angle of Attack and -90° Aileron Deflection.

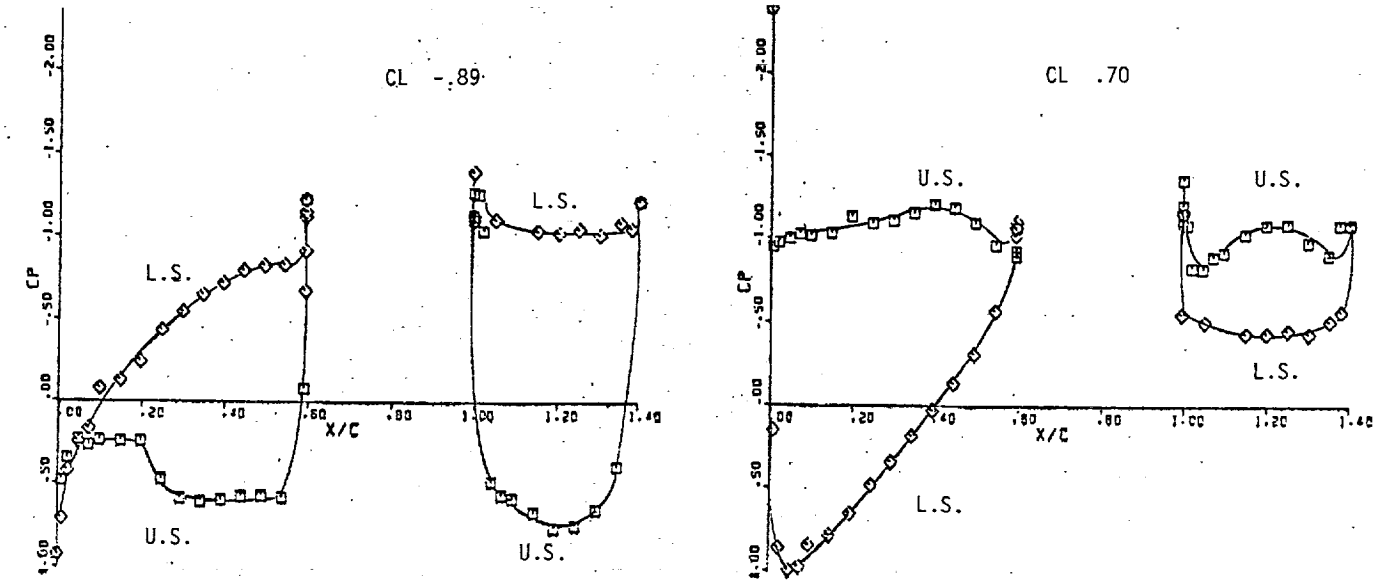

a) 18° Angle of Attack

b) 36° Angle of Attack

FIGURE 10. Pressure Distribution of 0.38c Plain Aileron at 18° and 36° Angle of Attack and -90° Aileron Deflection.

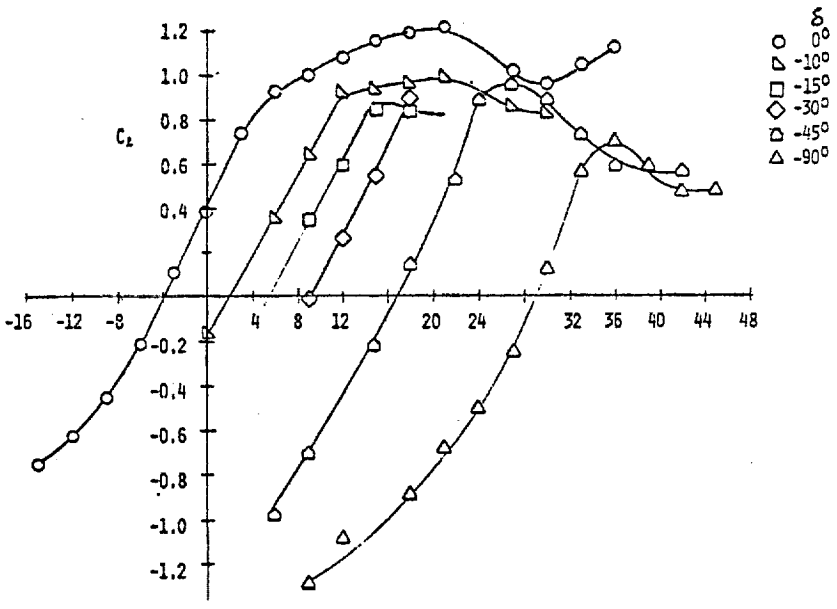

a) Lift Coefficient
vs
Angle of Attack

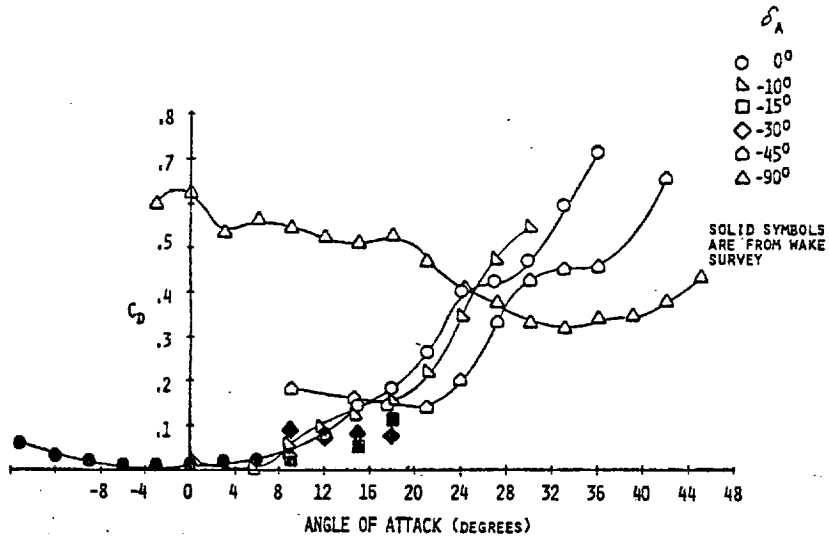

b) Drag Coefficient
vs
Angle of Attack

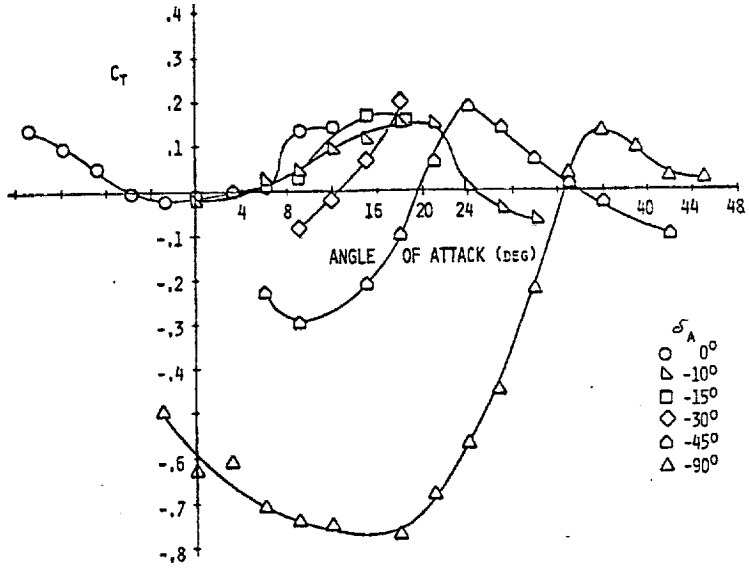

c) Thrust Coefficient
vs
Angle of Attack

FIGURE 11. Aerodynamic Characteristics of the 0.38c Plain Aileron at M = 0.25 and Re = 5 x 10^6.

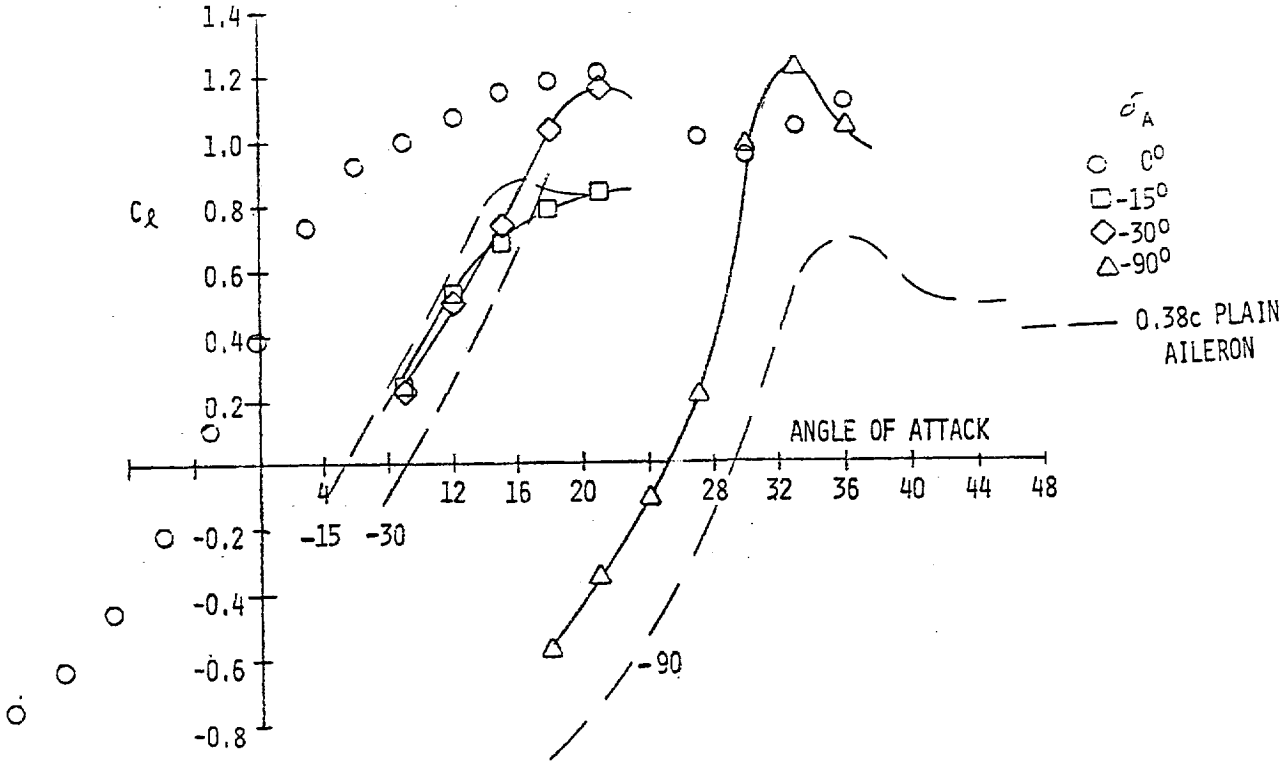

a) Lift Coefficient vs Angle of Attack

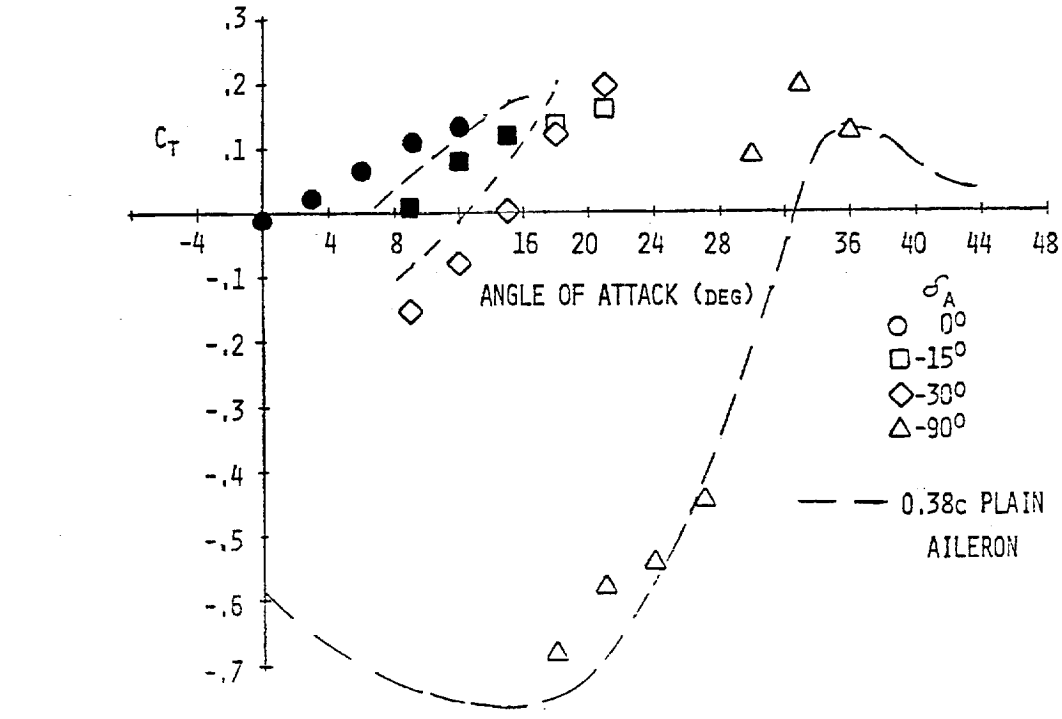

b) Thrust Coefficient vs Angle of Attack

FIGURE 12. Lift and Thrust Coefficients of the 0.38c Balanced Aileron.

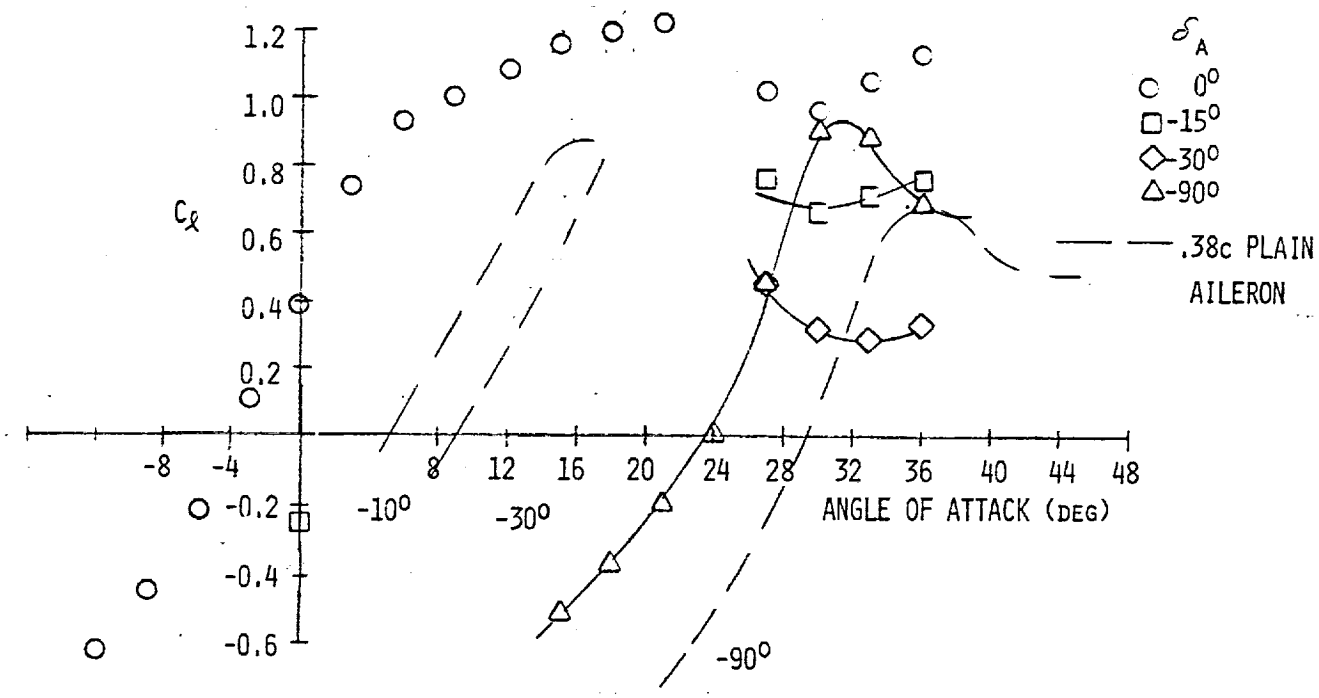

a) Lift Coefficient vs Angle of Attack

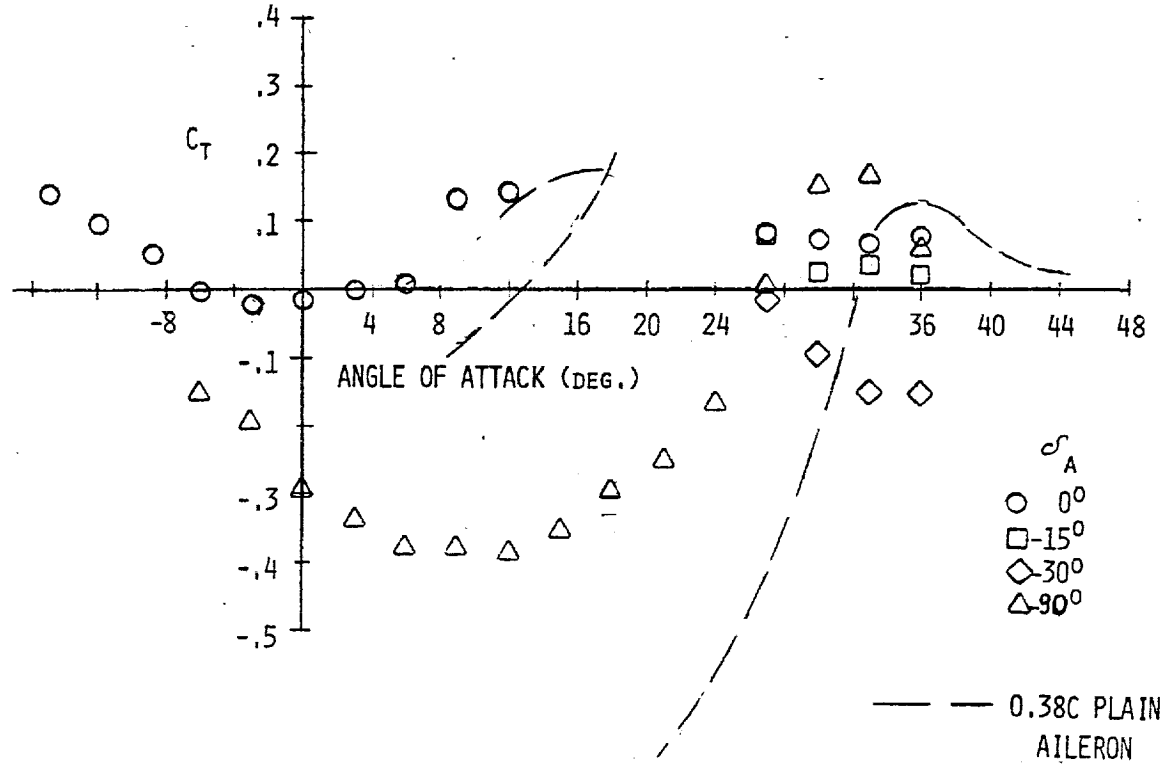

b) Thrust Coefficient vs Angle of Attack

FIGURE 13. Lift and Thrust Coefficients of the 0.30c Plain Aileron.

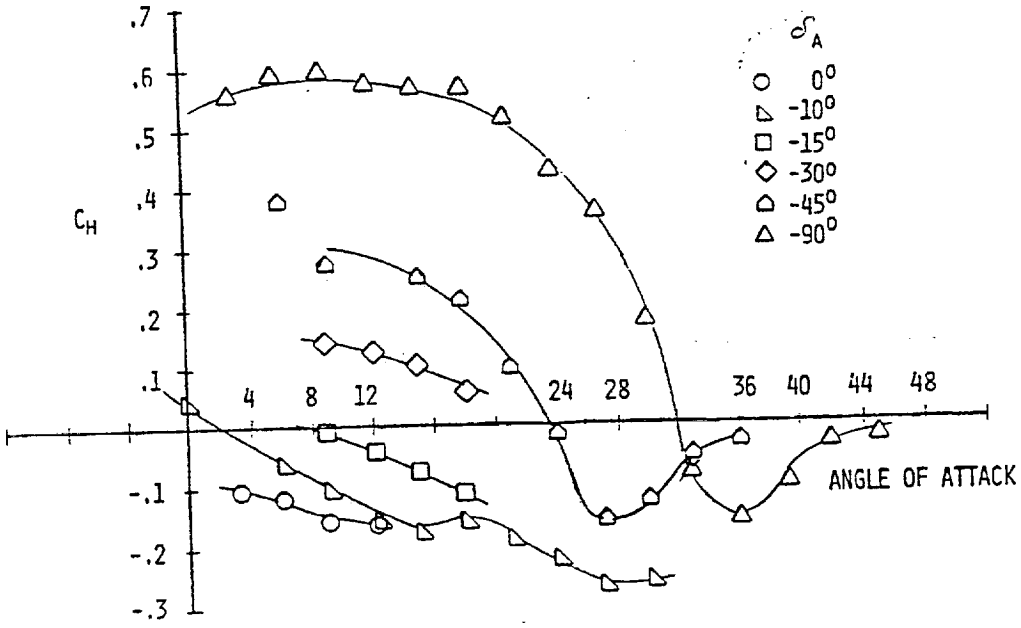

FIGURE 14. Hinge Moment Coefficient vs. Angle of Attack for the 0.38c Plain Aileron.

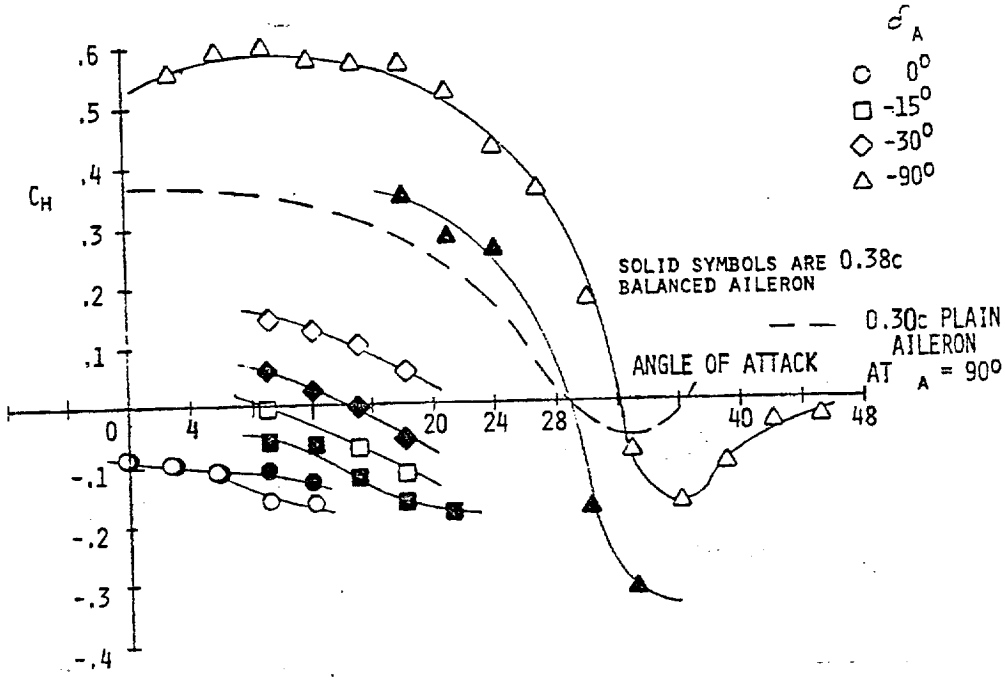

FIGURE 15. Hinge Moment Comparisons for the 0.30c Plain and 0.38c Balanced Aileron.

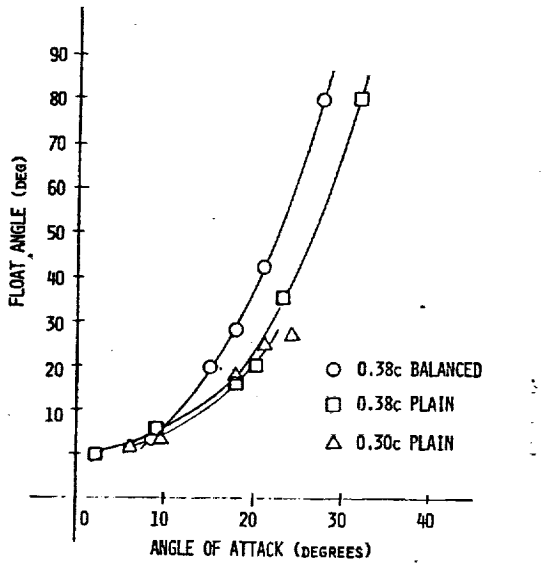

FIGURE 16. Angle for Zero Hinge Moment vs Angle of Attack